Document Version
Final published version

Citation (APA)

Using acoustic emission monitoring to assess the reliability of existing concrete structures: a case study

Fengqiao Zhang

Department of Engineering Structure, Delft University of Technology, the Netherlands, F.Zhang-5@tudelft.nl
....

Abstract

This study explores the use of Acoustic Emission (AE) monitoring to evaluate the structural reliability of existing concrete structures during load testing. AE data were processed probabilistically to estimate crack locations and, combined with the strut-and-tie model, were used to assess shear resistance. Based on the processed AE data, a probabilistic framework was implemented to assess the structural reliability. The results demonstrate that incorporating AE significantly reduces the required load levels for indicating specific reliability index while maintaining safety during load testing. This research highlights the potential of AE as an efficient tool for reliability assessment of existing concrete structures.

Keywords

concrete structures, reliability assessment, structural resistance, Acoustic Emission monitoring

1 Introduction

Many existing concrete structures are approaching the end of their service life [1], raising concerns about their safety [2]. Structural reliability assessment is important to ensure safety and provides useful information for decision making such as maintenance [3]. However, in existing concrete structures, many design parameters are unknown, and material properties and load conditions may change over time [4, 5]. These uncertainties and incomplete information challenge the reliability assessment.

Structural health monitoring (SHM) can provide up-to-date information for structural reliability analysis. Various sensing technologies—including linear variable differential transformers (LVDTs), digital image correlation (DIC), fibre optic sensors (FOS), acoustic emission (AE) sensors, and accelerometers—can capture important structural parameters such as deflection, strain, stress, crack location, and crack width [6].

In SHM, various sources of uncertainty must be considered, including sensor placement, data recording, and signal processing algorithms [7]. Aleatory uncertainties (e.g., random noise) are irreducible but can be mitigated using statistical techniques, while epistemic uncertainties (e.g., biases due to model error) are reducible through proper calibration and validation [8]. Understanding and incorporating these uncertainties into the monitoring framework would improve the reliability of structural assessments.

With SHM information, the load and resistance models can be updated to predict the structural performance under different load scenarios [9]. Load models describe forces acting on the structure (dead loads, live loads, environmental loads such as wind or seismic), while resistance models estimate the capacity of a structure or its components to withstand loads without failure [10]. The resistance of structural components is influenced by factors such as material strength, member dimensions, and degradation due to environmental exposure or mechanical wear. These parameters exhibit variability, necessitating a probabilistic treatment.

By integrating monitoring-informed resistance and load distributions, the reliability index (β) can be dynamically calculated [11]. Time-dependent reliability analysis projects future risks by combining degradation models (e.g., carbonation progression) with anticipated load changes (such as increased traffic or climate-driven extremes) [4]. A Bayesian framework can be implemented to systematically combine prior knowledge with new SHM data. The process begins with a prior analysis using existing data as a baseline for reliability assessment. Monitoring data are then incorporated through a likelihood function, quantifying discrepancies between observed and predicted performance. This ensures model predictions are aligned with real-world observations. Posterior updating refines the model parameters

based on the combined prior information and new data. This iterative process enables continuous improvement of the reliability index, making it more representative of the actual structural condition.

A Bayesian framework has been developed to incorporate DIC crack width measurement in the structural reliability assessment [12]. Compared to DIC, AE monitoring has a different underlying physics, resulting in more sensitive crack detection [13] and the ability to detect the internal damages [14]. Therefore, incorporating AE information for the structural reliability assessment can be beneficial.

This paper extends the Bayesian framework originally developed for DIC-based reliability assessments to incorporate AE data. It accounts for uncertainties across the load and resistance models, including the AE-based shear failure indicators. During load testing of a full-scale reinforced concrete beam without shear reinforcement, the minimum annual reliability for disapproval of existing structures ($\beta = 4.0$) can be demonstrated at a lower load level when AE information is incorporated. This approach reduces the need for excessive loading, enhancing both cost efficiency and safety in load testing.

2 Using acoustic emission to calculate the structural reliability

2.1 From data to information: probability density of AE events

Sudden changes in concrete (such as cracking) release energy in the form of acoustic emissions, which propagate as elastic waves through the concrete and can be detected by AE sensors [15]. Based on the arrival times of the AE signals at multiple sensors and the sensor locations, AE source localization methods can estimate the position of the source event [16].

Uncertainties in the localization process can cause errors in the identified source position [17]. These uncertainties arise from factors such as arrival-time picking errors, wave propagation variations (e.g. the presence of cracks between source and sensors), or sensors missing weak signals due to large spacing. Through numerical and experimental studies, the source localization error was found to follow a chi distribution. Based on the quantified error, a probabilistic source localization method was developed in a previous paper [18]. A parameter called probability density of AE events (pdAE) is computed, which incorporates the localization uncertainties and represents the probability that an AE event originated at a given location in the structure:

$$p_{\mathbf{A}}(\mathbf{x}) = \sum_{a \in \mathbf{A}} f(x, x_{g,a}) = \sum_{a \in \mathbf{A}} \frac{1}{\left(\sqrt{2\pi}\right)^k} \frac{1}{\sigma^k} e^{-\|x - x_{g,a}\|^2 / 2\sigma^2} , k \in \{1,2,3\} \tag{1}$$

where $\mathbf{A}$ is a set of all AE events that occurred in the measuring time and space range, $\mathbf{x}_{g,a}$ is the estimated location of event a, $\mathbf{x}$ is a random point in the space of k dimensions (in this paper, 2D source localization is performed, thus $k = 2$) and σ is the standard deviation of the source localization error component (this paper takes $\sigma = 55$mm [18]). By including the source localization errors, the computed parameter pdAE can more clearly identify the location of cracks.

Figure 1a shows an example of AE source locations estimated using a conventional localization method, in comparison with the actual crack pattern (the real crack is indicated by the white line). Each dot represents a localized AE source. Due to localization errors, many AE source points deviate significantly from the actual crack, resulting in an unclear indication of the crack path.

Figure 1b shows the pdAE field for a single AE event. The estimated source location for this event is at (2.48, 0.35) m, and points closer to that location have a higher probability of being the true source. By superimposing the pdAE fields of multiple events. Figure 1c shows the pdAE field for all AE events from Figure 1a. By accounting for the source localization uncertainty, the crack location is more clearly identified; even a secondary crack near the main crack becomes distinguishable.
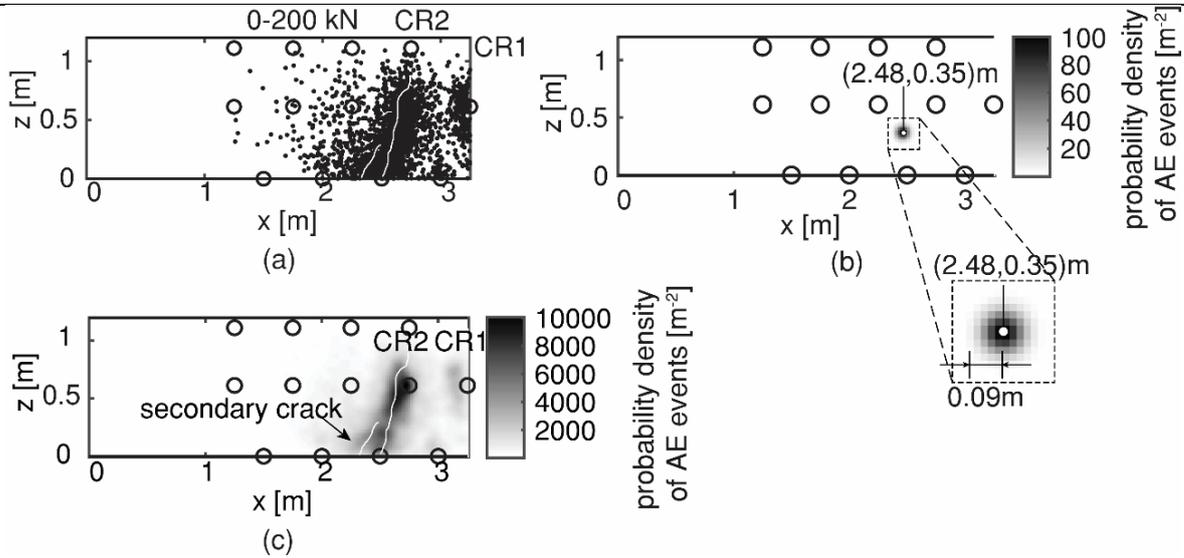
Figure 1 From 0 to 200 kN (excluding AE events during unloading) in test I123A: (a) estimated source locations with marked actual crack pattern, (b) the pdAE field of one AE event, (c) the pdAE field of all AE events with marked actual crack pattern [18].

2.2 From information to structural resistance: AE-based shear failure indicators

During the shear failure of reinforced concrete beams without shear reinforcement, the integrity of the concrete strut (the diagonal compression region) is found closely linked to the remaining shear resistance. In a previous paper [19], a set of indicators have been proposed which use pdAE data to evaluate the integrity of this strut region. Three levels of structural damage in a beam under shear are identified (illustrated in Figure 2).

- **Initial flexural cracking – Green light:** When the pdAE in the tie region first reaches the predefined threshold, a flexural crack has been opened; this is the green-light criterion.

- **First strut cracking – Yellow light:** When the pdAE in the strut region reaches the same level as that recorded at the green-light criterion, a crack has reached the strut; this is defined as the yellow-light criterion.

- **Critical shear crack – Red light:** When the pdAE in the strut exceeds the maximum accumulated pdAE observed in the tie region, the strut is considered heavily damaged (approaching failure). This condition, caused by a significant increase in shear crack opening/displacement, is defined as the red-light criterion.
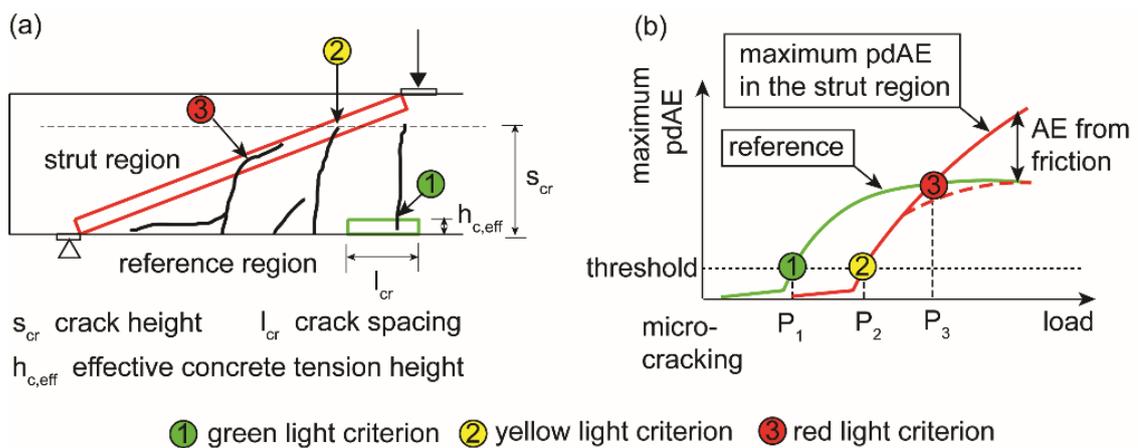

Figure 2 The traffic light system for shear failure indication: (a) cracking behaviour at the criteria and (b) determination of the criteria by comparing the maximum pdAE in the strut and the reference region.

The proposed traffic-light system was validated with shear tests on reinforced concrete beams under various configurations. Description on the test series can be found in [19]. One of these tests, i.e. I123A, was used in this paper to demonstrate the reliability assessment as described in Section 3.

For a traffic light criterion i, the shear resistance factor $X_{AE,i}$, which is the ratio between the shear resistance and the shear effect of applied load and self-weight, is computed for the cross section at a distance of 1 m from the supporting line. Table 1 shows the shear resistance factor $X_{AE,i}$ in the six texts. At the green-light criterion ($i = 1$), the shear resistance factor was between 1.50 and 1.88. At the yellow-light criterion ($i = 2$), the shear resistance factor was between 1.13 and 1.75. At the red-light criterion ($i = 3$), the shear resistance factor is between 1.00 and 1.65, which is close to structural failure. Figure 3 shows that the shear resistance factor may increase with the shear span ratio.

Table 1 Shear resistance factor at the three criteria in the beam tests.

Beam test	Shear span ratio a/d	Shear resistance factor at green light $X_{AE,1}$	Shear resistance factor at yellow light $X_{AE,2}$	Shear resistance factor at red light $X_{AE,3}$
I123A	2,61	1.54	1.13	1.07
H601A	3,89	1.83	1.58	1.18
H602A	3,89	1.88	1.75	1.65
H603A	2,59	1.87	1.29	1.15
H604A	3,02	1.50	1.25	1.00
H853A	2,61	1.63	1.30	1.30
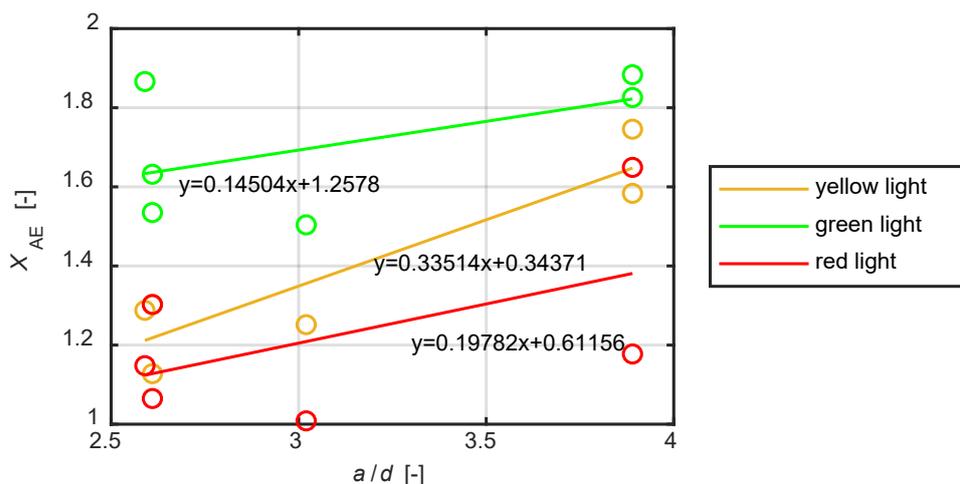
Figure 3 Shear resistance factors at different shear span ratio.

2.3 Reliability calculation

A Bayesian framework was applied, which facilitates the computation of limit state functions and systematically incorporates AE data. The method was originally developed to incorporate DIC crack width measurement [12]. This paper uses this framework to integrate AE-based indicators in the reliability assessment.

2.3.1 Limit state functions at different stages

The limit state function plays a central role in structural reliability assessment. The general format of limit state function is:

$$Z = \theta_R R - \theta_E E \tag{2}$$

where θ_R is the uncertainty associated with resistance calculation, R is the resistance, θ_E is the model uncertainty of the load effect calculation, E is the load effect. For concrete bridges in service, the load effect is

$$E = G_{DL} + G_{SDL} + C_{0Q}Q \tag{3}$$

where G_{DL} is the dead load effect, G_{SDL} is the superimposed dead load effect, C_{0Q} is the time-invariant part of the live load effect, and Q is the time variant part of the traffic load effect.

The resistance of existing structures R may have high uncertainty due to limited available information. Instead of using a purely theoretical resistance model, the resistance R is estimated by integrating in-situ measurements with insights from laboratory experiments and analytical modelling. This data-informed approach also influences the estimation of θ_R (since the uncertainty in the resistance prediction is reduced by testing information).

Without any AE monitoring information, one can assume that the resistance of the tested structure must be at least sufficient to carry the dead load and the applied test load. The corresponding limit state function (including model uncertainties) only based on the applied load (baseline) can be written as:

$$Z_{LT,baseline} = \theta_R\big(\theta_E G_{DL} + \theta_{E,LT}Q_{LT}\big) - \theta_E\big(G_{DL} + G_{SDL} + C_{0Q}Q\big) \tag{4}$$

where Q_{LT} is the effect of the applied load, $\theta_{E,LT}$ is the model uncertainty of the load effect pertaining to the load testing situation. Model uncertainty in the load test ($\theta_{E,LT}$) is likely correlated to that in the regular load, due to similar load application methods, test configurations, and failure modes.

With AE monitoring information, the resistance is estimated as the load effect (of applied load and self-weight) multiplied by the factor X_{AE}. The corresponding limit state function after load testing with the information from AE is then:

$$Z_{LT,AE} = \theta_R X_{AE}\big(\theta_E G_{DL} + \theta_{E,LT}Q_{LT}\big) - \theta_E\big(G_{DL} + G_{SDL} + C_{0Q}Q\big) \tag{5}$$

2.3.2 AE-based shear resistance factor in the load testing

The shear resistance factor $X_{AE,p}$ for an applied load p is computed as:

$$X_{AE,p} = \begin{cases} X_{AE,1} & p \leq P_1 \\ X_{AE,2} & P_1 < p \leq P_2 \\ X_{AE,3} & P_2 < p \leq P_3 \end{cases} \tag{6}$$

where the load P_i corresponds to when the traffic light i is observed, $i = 1$ represents green light, $i = 2$ represents the yellow light, and $i = 3$ represents the red light.

In this approach, the resistance factor for any applied load is set to the value of the next traffic-light criterion. For example, before reaching the green-light criterion, no acoustic emissions (AE) from cracking are detected, indicating that the load effect is lower than at the green-light level. Consequently, the actual resistance factor would be higher than the one assigned at the green-light criterion.

In other words, Equation (7) generally assigns a lower resistance factor across most load levels. A lower resistance factor leads to an underestimation of shear resistance, with the effect being more pronounced when the load level is significantly lower than the upcoming traffic-light criterion. Notably, once the red-light criterion is reached, the shear resistance factor is no longer computed, as the structure is considered near failure.

2.3.3 Bayesian update

During testing, information of successful carrying an applied load is incorporated into a Bayesian updating scheme to refine the joint posterior distribution $\boldsymbol{\theta}$ (θ_R, X_{AE}):

$$p\big(\boldsymbol{\theta}\big|Z_{LT,during\ test} > 0\big) \propto p\big(Z_{LT,during\ test} > 0\big|\boldsymbol{\theta}\big)p(\boldsymbol{\theta}) \tag{7}$$

where $Z_{LT,during\ test} = \theta_R X_{AE}\big(\theta_E G_{DL} + \theta_{E,LT}Q_{LT}\big) - \big(\theta_E G_{DL} + \theta_{E,LT}Q_{LT}\big) \propto \theta_R X_{AE} - 1$, which is the limit state function during loading.

In mathematical terms, the likelihood of survival $p\big(Z_{LT,during\ test} > 0\big|\boldsymbol{\theta}\big)$ serves as an indicator function that filters the prior distribution $p(\boldsymbol{\theta})$. In a Monte Carlo simulation, this involves discarding samples that do not satisfy $Z_{LT,during\ test} > 0$, effectively distinguishing between parameter realizations that would fail and those that would survive the applied load. Then the Markov Chain Monte Carlo sampling [20] is used to efficiently draw samples from the posterior distribution of $\boldsymbol{\theta}$ given this survival event. In Bayesian inference, the factor X_{AE} is described by a Student's *t*-distribution which is mathematically equivalent to assuming a non-informative prior on the parameters of normal distribution. This approach provides a convenient way to update the distribution of X_{AE} (and θ_R) without introducing bias, reflecting only the information gained from the successful load test.

Once updating is performed, the revised parameters θ_R' and X_{AE}' are used in the limit state function $Z_{LT,AE}$ in Equation (6).

3 Case study

3.1 Test description

The case study focuses on evaluating structural reliability in shear for a typical reinforced concrete slab bridge constructed in the 1960s. This type of structure has limited shear reinforcement and is thus vulnerable to shear failure. To simulate such a bridge, a concrete beam (a slab strip) of 0.3 m width, 10 m length, and 1.2 m height was cast in the laboratory. Figure 4 shows the beam configuration, including dimensions, reinforcement layout, supports, and loading points. The concrete strength class was C65, assuming that bridges originally built with C35 concrete in 1960s have increased in strength over time. In total, six beams were tested, names as I123A, H601A, H602A, H603A, H604A and H853A. Details of the test setup can be found in a previous paper [19].The test I123A is used in this paper to demonstrate the reliability assessment in the load testing.

The beam was loaded in the lab until shear failure occurred. The ultimate load capacity (P_u) was 300 kN. AE monitoring was conducted throughout the load test. According to the defined AE-based indicators (the maximum pdAE in the strut region), the green-light, yellow-light, and red-light criteria were reached at load levels of 180 kN, 250 kN, and 290 kN respectively. These load levels indicate the points at which the first flexural crack formed (green), the first shear crack reached the strut (yellow), and the strut was critically damaged (red) during the test.
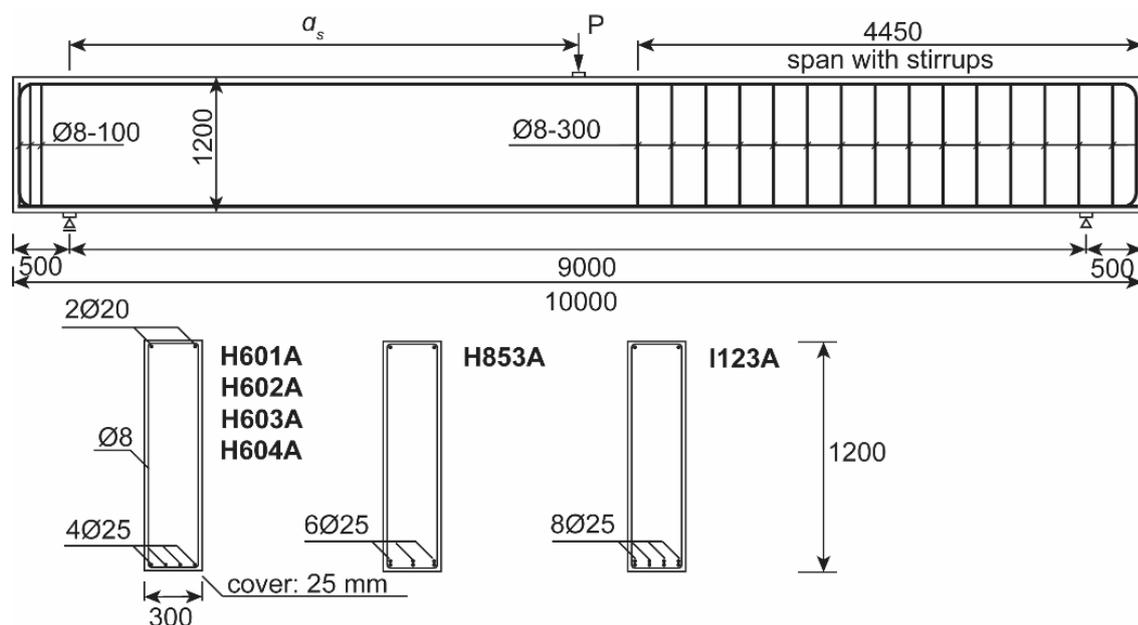

Figure 4 A sketch of beam configuration including beam dimension, reinforcement layout and locations of supports and load [21].

3.2 Probabilistic models

To perform the reliability update, a probabilistic model tailored to the test structure was developed. The mean values and coefficients of variation (COV) of the random variables (see Table 2) are taken from a previous study [12] which were based on recommendations from the JCSS Probabilistic Model Code [22], fib Bulletin 80 [10], and specifications on the Weigh-In-Motion (WIM) traffic loads [23].

The load effect is assessed at a cross-section located 1 m from the support line. It should be noted that the mean values for dead load effect G_{DL}, superimposed load effect G_{SDL} and traffic load effect Q are estimated to be one twelfth of the load effect applied in the previous study [12], considering that the slab width in the previous study (3.6 m) is twelve times the strip width in this paper (0.3 m). Here the load effect is assumed to be uniformly distributed in the width direction.

The mean value and covariance of X_{AE} take the values in Table 1. For yellow-light criterion, the mean and covariance of $X_{AE,2}$ at the $a/d = 2.61$ is used (which is the shear span to depth ratio of the investigated beam I123A).

Table 2 Overview of random variables in the limit state function

	Random variables in the limit state function	Distribution	Mean	Covariance
θ_R	Model uncertainty of the resistance	Lognormal	1	0,15
$X_{AE,p}$	Resistance factor for green light $X_{AE,1}$ (when the applied load $p \leq = 180$ kN)	Student's t	1.64	0,11
	Resistance factor for yellow light $X_{AE,2}$ (when the applied load 180 kN $< p \leq 250$ kN)	Student's t	1.22	0.10
	Resistance factor for red light $X_{AE,3}$ (when the applied load 250 kN $< p \leq 290$ kN)	Student's t	1.13	0,22
G_{DL}	Dead load effect	Normal	29.7kN	0,05
G_{SDL}	Superimposed load effect	Normal	4.9kN	0,1
Q	Traffic load effect	Gumbel	32.5kN	0,035
C_{0Q}	Time-independent uncertainty of traffic load effect, including dynamic effect	Lognormal	1,1	0,1
Q_{LT}	Load effect by the load testing	Normal	varies	0.02
θ_E	Model uncertainty of load effect	Lognormal	1	0,1
$\theta_{E,LT}$	Model uncertainty of load test effect; correlation $\rho(\theta_E, \theta_{E,LT})=0.7$	Lognormal	1	0,1

3.3 Reliability calculation results

Figure 5 compares the distribution of shear resistance with and without AE information when loaded to 90 kN. The results show that resistance estimated using AE data was approximately 1.65 times higher (146.87/88.78) than without AE, with a wider distribution. This corresponds to the applied resistance factor at the green-light criterion. The incorporation of AE data confirmed a greater structural resistance, leading to a higher reliability index.

Figure 6 shows the reliability index at all load levels, including results with and without AE information after successful loading, as well as results during the loading process. The minimum annual reliability index for disapproval of existing bridges is $\beta = 4.0$, according to NEN 8700 [24]. With AE monitoring data, the bridge was informed to reach the required reliability index of 4.0 when loaded to 90 kN. Without incorporating AE data, the same level of reliability would only be confirmed after loaded to 170 kN. Using AE allowed the load test to be stopped at a lower load while still confirming that the structure met the reliability requirement.

The reliability index during the load testing itself provides insight into the risk associated with applying the load. At 110 kN when AE results showed sufficient structural reliability level ($\beta > 4.0$), the reliability index during the load testing was around 2, corresponding to a failure probability of 2.3%. This relatively high probability of survival confirms that the structure was likely to endure the applied load without failure. At 170 kN when the baseline showed same level of structural reliability, the reliability during the load testing was a bit lower, around 1, meaning a higher failure probability of 16%. The reliability index during load testing was updated at each increment of the load, enabling continuous assessment of risk as the load increased.
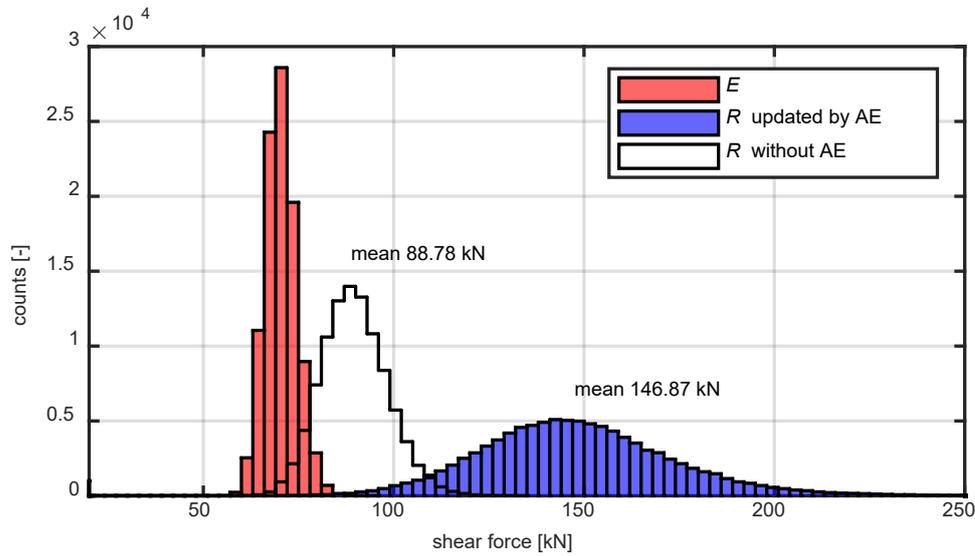
Figure 5 The distribution of the load effect, estimated resistance without AE (baseline), and estimate resistance updated by AE at the load level of 90 kN.
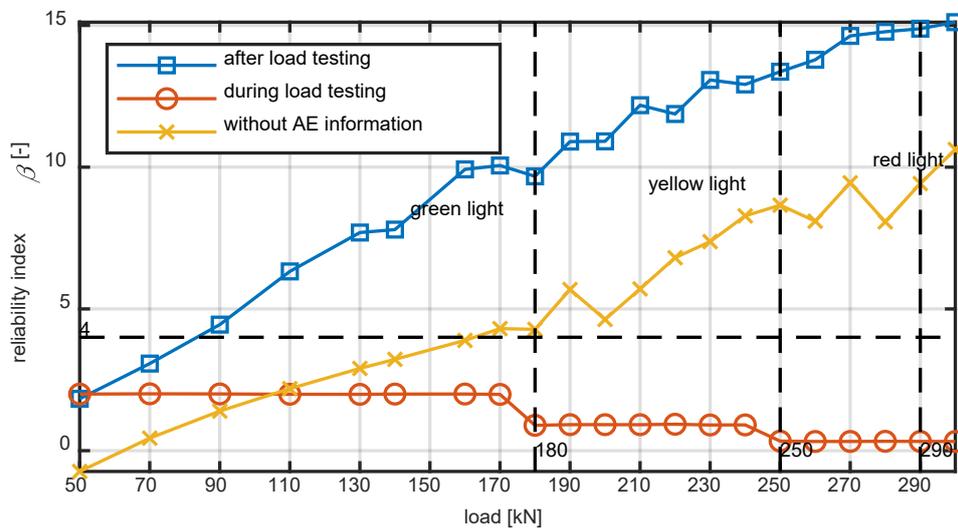

Figure 6 Comparison of reliability index after load testing updated by AE, during load testing updated by AE and without AE information.

4   Discussions

This study extends the probabilistic framework which was developed to incorporate DIC crack width data for reliability assessment [12] to the AE application. By integrating AE monitoring into the probabilistic approach, this study shows the potential of AE to provide early warning indicators of structural reliability while reducing reliance on high-load testing.

Compared to the previous research on using DIC crack width as information, a key advantage of AE monitoring is its ability to detect fine cracking, particularly microcracking, before it becomes visually apparent. However, AE data interpretation remains a challenge due to inherent uncertainties in source localization and noise influence. Future improvements can focus on improving uncertainty quantification methods to increase the robustness of AE-based assessments.

Moreover, the extension to incorporate AE data highlights the flexibility of the probabilistic framework. Future work could incorporate data from various sources (e.g., traffic-induced vibrations, temperature effects). And multiple structural resistance models could be used such as finite element model (FEM). To properly incorporate them into the reliability framework, uncertainties and correlations among various data/models need to be quantified.

Furthermore, the current study is based on controlled laboratory experiments, which provide a well-defined environment for evaluating monitoring-based reliability assessment. However, practical implementation on in-service structures requires further validation. Factors such as environmental noise and variable boundary conditions in real bridge slabs must be accounted for.

5   Conclusions

This study extends an existing crack width-based framework for structural reliability assessment to AE application. The introduction of the probability density field of AE events (pdAE) allows for more accurate crack identification, while the AE-based 'traffic light' failure indicators provide a computationally efficient structural resistance model.

The case study highlights the significant value of AE information in reliability updating. The results indicate that incorporating AE data allows structural reliability to be verified at lower load levels compared to traditional load testing, thereby reducing the risk of unnecessary overloading. Moreover, Bayesian updating techniques enable continuous reliability assessments during loading.

Despite the promising results, further research is needed to validate the framework under real-world conditions. Future work should focus on refining AE monitoring plans and data processing, integrating complementary SHM techniques, and improving probabilistic models for reliability updating.

Acknowledgements

References

1. Rijkswaterstaat, *Staat van de Infra RWS*. 2021, Rijkswaterstaat: the Netherlands.
2. Fischer, O., et al., *Nachrechnung von Betonbrücken - Systematische Datenauswertung nachgerechneter Bauwerke Re-analysis of concrete bridges*. Berichte der Bundesanstalt für Straßenwesen, Reihe B: Brücken- und Ingenieurbau - 124. 2016.
3. Rijkswaterstaat, *RTD 1006 Richtlijnen Beoordeling Kunstwerken (RBK)*. 2022.
4. de Vries, R., et al., *Time-dependent reliability assessment of existing concrete bridges with varying knowledge levels by proof load testing.* Structure and Infrastructure Engineering, 2024. **20**(7-8): p. 1053-1067.
5. Walraven, J. and G. Dieteren, *Assessment of existing structures in fib modelcode 2020: Solutions and examples.* Structural Concrete, 2023. **24**(4): p. 4424-4432.
6. *fib, Bulletin 22: Monitoring and safety evaluation of existing concrete structures*. 2003.
7. Kamariotis, A., et al., *On the Consistent Classification and Treatment of Uncertainties in Structural Health Monitoring Applications.* ASCE-ASME J Risk and Uncert in Engrg Sys Part B Mech Engrg, 2024. **11**(1).
8. Kiureghian, A.D. and O. Ditlevsen, *Aleatory or epistemic? Does it matter?* Structural Safety, 2009. **31**(2): p. 105-112.
9. Okasha, N.M., D.M. Frangopol, and A.D. Orcesi, *Automated finite element updating using strain data for the lifetime reliability assessment of bridges.* Reliability Engineering & System Safety, 2012. **99**: p. 139-150.
10. *fib, Bulletin 80: Partial factor methods for existing concrete structures*. 2016: Lausanne, Switzerland.
11. Caspeele, R., W. Botte, and E. Vereecken, *Bayesian performance assessment of existing concrete structures combining different types of information from inspections and monitoring.* Structure and Infrastructure Engineering, 2025: p. 1-17.
12. de Vries, R., et al., *Structural reliability updating on the basis of proof load testing and monitoring data.* Engineering Structures, 2025. **330**: p. 119863.
13. Zhang, F., et al., *Monitoring Shear Behavior of Prestressed Concrete Bridge Girders Using Acoustic Emission and Digital Image Correlation.* Sensors, 2020. **20**(19): p. 5622.
14. Zhang, F., Y. Yang, and M.A.N. Hendriks, *Identification of internal damages in reinforced concrete slabs using probability density field of acoustic emission events*, in *35th European and 10th International Conference on Acoustic Emission Testing*. 2022: Ljubljana, Slovenia. p. 310-318.

15. Grosse, C. and M. Ohtsu, *Acoustic emission testing: Basics for Research-Applications in Civil Engineering*. 2008. 1-404.
16. Kundu, T., *Acoustic source localization.* Ultrasonics, 2014. **54**(1): p. 25-38.
17. Zhang, F., L. Pahlavan, and Y. Yang, *Evaluation of acoustic emission source localization accuracy in concrete structures.* Structural Health Monitoring, 2020. **19**(6): p. 2063-2074.
18. Zhang, F., et al., *Probability density field of acoustic emission events: Damage identification in concrete structures.* Construction and Building Materials, 2022. **327**: p. 126984.
19. Zhang, F., Y. Yang, and M.A.N. Hendriks, *Acoustic emission-based indicators of shear failure of reinforced concrete beams without shear reinforcement.* Engineering Structures, 2025. **330**: p. 119929.
20. Hastings, W.K., *Monte Carlo Sampling Methods Using Markov Chains and Their Applications.* Biometrika, 1970. **57**(1): p. 97-109.
21. Zhang, F., Y. Yang, and M.A.N. Hendriks, *Investigation of concrete crack kinematics through probability density field of the location of acoustic emission events.* Construction and Building Materials, 2023. **400**: p. 132595.
22. Joint Committee on Structural Safety (JCSS), *Probabilistic Model Code*. 2001.
23. de Vries, R., et al., *Proof Load Testing Method by the American Association of State Highway and Transportation Officials and Suggestions for Improvement.* Transportation Research Record, 2023. **2677**(11): p. 245-257.
24. Nederlands Normalisatie-instituut (NEN), *NEN 8700: Beoordeling van de constructieve veiligheid van een bestaand bouwwerk bij verbouw en afkeuren – Grondslagen*. 2011.